UDK 621.979.1
Original scientific article/Izvirni znanstveni članek

ISSN 1580-2949
MTAEC9, 57(3)267(2023)

DEVELOPMENT OF A PNEUMATIC, ARTIFICIAL-MUSCLE-BASED PRESS FOR PUNCHING THIN METAL SHEETS

RAZVOJ STISKALNICE Z UMETNIMI PNEVMATSKIMI MIŠICAMI ZA TANKOSTENSKO PREBIJANJE TANKIH KOVINSKIH PLOČEVIN

Akin Oguz Kapti[1,2] *, Ilker Atakul[1]

[1]Sakarya University, Mechanical Engineering Department, 54050, Sakarya, Türkiye
[2]Sakarya University Research, Development and Application Center, 54050, Sakarya, Türkiye

Prejem rokopisa – received: 2023-02-01; sprejem za objavo – accepted for publication: 2023-04-05

doi:10.17222/mit.2023.783

The present study examines the nonlinear behavior of pneumatic, artificial muscles and investigates their availability for producing pressing forces over the experimentally determined tensile forces. It covers the design and manufacturing studies of a test setup and a pneumatic, artificial-muscle-based press to achieve this goal. The press design consists of a single pneumatic artificial muscle to provide the main pressing force and another two to bring the press back to the neutral position. The proposed approach is considered sufficient for thin sheet-metal punching molds and fills a gap in the spectrum of pressing technologies. A sufficient level of pressing force for thin sheet-metal punching is found to be achievable using a single 40-mm-diameter, pneumatic, artificial muscle. The results show that the press can produce (9.1, 23.1 and 36.9) kN pressing forces at (200, 400 and 600) kPa air pressures, respectively.

Keywords: pneumatic artificial muscle, table-top press, sheet metal, punching.

Predstavljeni so preizkusi nelinernegaobnašanja umetnih pnevmatskih mišic in raziskava možnosti izdelave stiskalnice na osnovi eksperimentalno določenih nateznih obremenitev. Za dosego želenega cilja so oblikovali napravo in njeno postavitev, analizirali možnosti za njeno izdelavo ter jo nato izdelali z ustreznimi umetnimi pnevmatskimi mišicami. Izdelana stiskalnica je imela eno umetno pnevmatsko mišico (napihljiv gumijast valj), ki je zagotavljala glavno silo stiskanja (kompresijo) in drugih dveh, ki sta stiskalnico vračali nazaj v nevtralni položaj. Ocenili so, da predlagani pristop omogoča prebijanje tankih kovinskih pločevin in s tem zapolnjuje vrzel oz. manjkajoče vrste stiskalnic za vrsto stiskalnih tehnologij. Ugotovili so, da je doseženaraven prebijalne sile dovolj velika za prebijanje tankih kovinskih pločevin pri uporabi ene umetne pnevmatske mišice premera 40 mm. Rezultati so pokazali, da s stiskalnico lahko dosežejo sile stiskanja velikosti (9,1in 23,1oz. 36,9) kN pri tlakih zraka (200, 400 oz. 600) kPa.

Ključne besede: umetna pnevmatska mišica, namizna stiskalnica, kovinska pločevina, prebijanje

1 INTRODUCTION

A pneumatic, artificial muscle (PAM) is a flexible tensile actuator that allows more precise motion and position control, where larger forces can be achieved with smaller powers than a pneumatic cylinder. It has been named muscle because it works similarly to the principle of the biological muscle, producing pulling force by contracting and shortening. It consists of a contractible cylindrical rubber diaphragm with a high force-to-weight ratio (400:1). This diaphragm, which is made of a pressure-resistant hose and strong rhomboid fibers, surrounds the working environment and provides an airtight seal. The working principle of the PAM is that the pneumatic pressure acting over the entire inner surface forces the cylindrical structure to be spherical and thus creates a tensile force in the longitudinal direction.

PAM has many outstanding features. It has the properties of a high force-to-weight ratio, structural flexibility, lightness, insensitivity to dirt (abrasive particles, dust, etc.), a hermetically sealed structure, and ease of handling. The pulling force produced by a PAM in its initial position reaches up to ten times higher than that of a conventional pneumatic cylinder of the same diameter. It provides silent and precise positioning with pressure regulation, including intermediate positions. It enables large parts (side covers, plates, etc.) to be easily clamped. Due to its adjustable spring force and flexibility, a PAM can absorb the high stresses that occur when the films and papers are transported or wound using rollers. It does not need to be constantly connected to the compressed-air supply to function. It allows the amplitude and cycle rate to be adjusted independently of each other. No need for lubricant, as it does not contain any moving parts. On the other hand, there are also some disadvantages, such as the maximum 25 % of the stroke length being available, the reduction of the force to zero depending on the stroke, and the absence of double-acting operation availability.

PAMs have begun to attract attention again in recent years. In the literature, there are many PAM-based studies conducted in different application areas, such as a parallel manipulator designed using three PAMs,[1] a novel actuator for an underwater robot retrieving nuclear

*Corresponding author's e-mail:
aokapti@sakarya.edu.tr (Akin Oguz Kapti)

waste,[2] a search-type rescue robot,[3] an active vibration control system for a footbridge,[4] an underground explorer robot mimicking the peristaltic crawling of earthworms,[5] a crankshaft mechanism designed by using three PAMs for a small rubber-wheeled vehicle,[6] and mechanical actuation studies on PAMs that are driven by hydrogen-gas pressure provided by absorption of the metal hydride.[7–9] Robotics engineers have also begun to rediscover PAMs, and use them as robotic actuators and prosthetic assistive devices.[10] They are also promising for biomimetic-legged robots because of their adjustable stiffness, high power/weight ratio, and structural flexibility.[11] A biomimetic exoskeleton powered by an antagonistic pair of PAM for reliable actuation in orthopedic rehabilitation,[12] a two-link anthropomorphic arm constructed by PAMs for the upper-limb rehabilitation training,[13] a manipulator powered by PAMs for an exoskeleton application,[14] a robotic lower limb consists of a novel mechanism that is driven by a single PAM combined with a torsion spring for therapy robots,[15] and an assistive device for the agonist-antagonist actuation of the human forearm[16] can be mentioned as PAM-based studies focused on PAM behavior in robotic and prosthetic applications. The new type of bendable[17,18] or twistable[19] PAMs generating grasping or torsional motions for soft actuators also exist in the literature.

Despite the variety of applications mentioned above, a study in which PAMs are used to obtain pressing force has not been found in the literature. This study aims to experimentally measure the tensile force produced by PAMs at different air pressures and contraction rates and to examine their nonlinear behavior in a PAM-based press over the experimentally determined tensile forces. In this study the general structure of the PAM was investigated, and the design, manufacturing, and test studies of a PAM-based press actuated with three PAMs were carried out.

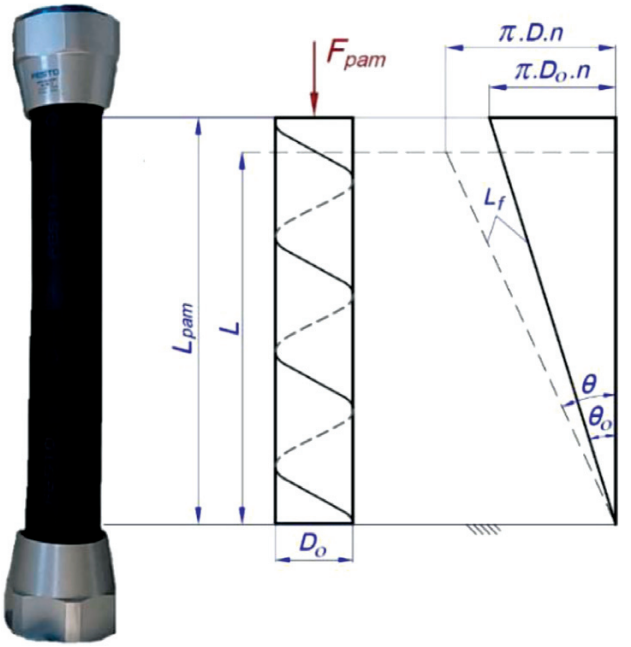

Figure 1: Basic dimensions and the force-generation model of the PAM

2 EXPERIMENTAL PART

2.1 Structure of the PAM

The basic dimensions and the force-generation model of the PAM are given in **Figure 1**. Basically, a PAM operates as a single-acting actuator against a pre-tensioning load. When pressure is applied, the pre-tensioned PAM contracts, shortens in length, increases in diameter, and produces a tensile force that nonlinearly depends on the contraction ratio, with optimum dynamic characteristics and minimum air consumption. The radial force produced by air pressure is converted to the tensile force on each non-extensible braided thread turning around the tube with a definite initial angle. This angle has an essential role in transforming the radial force into tensional force.

The initial length, the initial inner diameter, and the initial volume of the PAM can be expressed by Equations (1) – (3), respectively, as follows:

$$L_0 = L_f \cdot \cos\theta_0 \tag{1}$$

$$D_0 = \frac{L_f \cdot \sin\theta_0}{\pi n} \tag{2}$$

$$V_0 = \frac{L_f^3 \cdot \sin^2\theta_0 \cdot \cos\theta_0}{4\pi n^2} \tag{3}$$

where L_f, θ_o, and n are the length of rhomboid fibers, initial fiber winding angle, and the number of windings, respectively. To obtain the equation expressing the tensile force generated by a PAM, the first PAM's force characteristic model based on the principle of energy conservation was reconsidered by Chou and Hannaford.[20] In this model, the PAM force is expressed by Equations (4) – (6), respectively, as follows:

$$\frac{dV}{d\theta} = \frac{L_f^3 \cdot 2\sin 2\theta_0 \cdot \cos\theta_0 - \sin^3\theta_0}{4\pi n^2} \tag{4}$$

$$\frac{dL}{d\theta} = -L_f \cdot \sin\theta_0 \tag{5}$$

$$F_{pam} = -p\frac{dV}{dL} = p\frac{L_f^2 \cdot (3\cos^2\theta_0 - 1)}{4\pi n^2} = p\frac{\pi D_0^2}{4}\left(\frac{3\cos^2\theta_0 - 1}{1 - \cos^2\theta_0}\right) \tag{6}$$

The force obtained from Equation (6) is proportional to the air pressure and the initial cross-sectional area. The fiber-winding angle, which is 28.6° at the initial state,[21] increases up to 54.7° in the case of the minimum length and the maximum contraction, where the force is zero. The error between the measured and calculated force characteristic of the PAM is not negligible because the effects of the membrane's elasticity are entirely ne-

glected in the Schulte model. This model is insufficient as it allowed the correct calculation of the PAM's tensile force only in the case of the initial fiber angle. It was later developed by Tondu and Lopez[22] as follows:

$$F_{\text{pam}} = \frac{3pA_0^2}{\tan^2\theta_0}\left[1-(c_1\cdot e^{-p}+c_2)\left(\frac{L_0-L}{L_0}\right)\right]-\frac{pA_0^2}{\sin^2\theta_0} \quad (7)$$

where c_1 and c_2 are constants specified experimentally. Wickramatunge and Leephakpreeda[23] developed a new model supposing that the force characteristic of a PAM is equivalent to a mechanical spring with displacement and pressure-dependent spring stiffness. In their model, the pressure-dependent spring stiffness, shortening, and PAM force are expressed by Equations (8) – (10) as follows:

$$k = (c_3 p^2 + c_2 p\cdot\Delta L + c_1\Delta L^2 + c_0) \quad (8)$$

$$\Delta L = L-(h_2 p^2 + h_1 p + h_0) \quad (9)$$

$$F_{\text{pam}} = k\cdot\Delta L \quad (10)$$

where; c_0, c_1, c_2, c_3, h_0, h_1 and h_2 are constant coefficients specified experimentally. Considering the membrane's elasticity, Martens and Boblan[21] developed a PAM force model using Equations (11) – (12) as follows:

$$F_{\text{pam}} = p\frac{\pi D_0^2}{4}\left(\frac{3\cos^2\theta_0-1}{1-\cos^2\theta_0}\right)-E_{\text{ru}}\varepsilon_{\text{pe}}H_0\pi L\frac{\mathrm{d}D}{\mathrm{d}L}- \quad (11)$$
$$-E_{\text{ru}}\varepsilon_1 H_0\pi D$$

$$E_{\text{ru}} = c_3 L^3 + c_2 L^2 + c_1 L + c_0 \quad (12)$$

where E_{ru} is the modulus of elasticity of the membrane, ε_{pe} is the strain in the perimeter direction, ε_1 is the strain in the length direction, H_0 is the wall thickness of the membrane, and c_0, c_1, c_2 and c_3 are the constant polynomial coefficients specified experimentally.

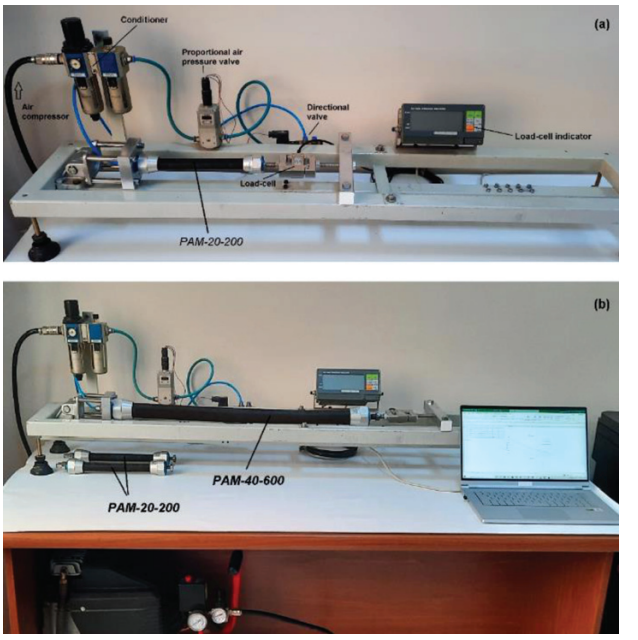

Figure 2: Test setups: a) PAM–20–200, b) PAM–40–600

2.2 Test setup

Figure 2 shows the experimental setup for the PAM's tensile force measurement. It consists of an air compressor, conditioner, directional valve, proportional air-pressure valve, and load cell. The main idea of the experiment is to measure the tensile force generated by the PAM at different contraction ratios and operating pressures. The proportional air-pressure valve adjusts the air pressure in the PAM, and the directional air valve manipulates the PAM connection between the compressor line and the atmospheric environment. The PAM length is fixed during the measurement with a length adjustment screw. The pressure is varied between the lower and up-

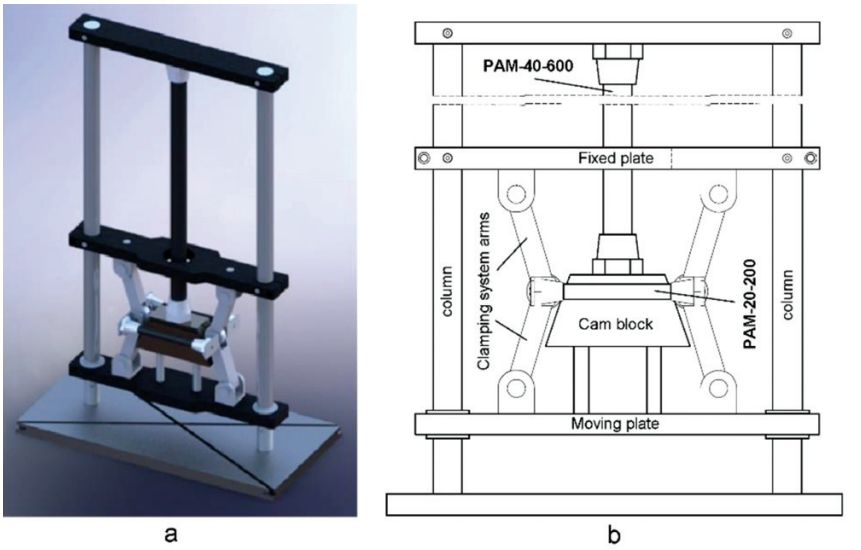

Figure 3: PAM-based press design: a) solid CAD model, b) schematic structure

per limits with intervals of 3.9 kPa, which is the accuracy of the proportional pressure valve. The tensile force of the PAM is measured by a load cell. The measurement process was repeated three times to reduce errors, and the force graphics are drawn according to the average values.

2.3 PAM-based press design

The solid CAD model and schematic structure of the developed press actuated with three PAMs are given in **Figure 3**. The press includes a clamping system consisting of articulated arms. This mechanism converts the pulling force produced by the single-acting PAM actuator into a pressing force. A cam block connected to the end of the PAM opens the arms of the clamping system. The PAM force is transmitted to the moving plate with the force-increasing reduction effect of the clamping system.

The main selection parameters of the PAM are the diameter and length. These parameters are defined as the initial inner diameter and visible muscle length between the connections in the non-pressurized and load-free state, respectively. The first one of the selected PAMs (PAM-40-600: 40 mm initial diameters and 600 mm initial lengths) provides the main press force, and the other two (PAM-20-200: 20 mm initial diameters and 200 mm initial lengths) return the press to the neutral position. The weight of the cam block makes up the pre-tensioning effect on the first one. The technical properties of the PAMs used are listed in **Table 1**.

Table 1: Technical properties of the PAMs used in the press design.

	PAM-20	PAM-40
Inner diameter	20 mm	40 mm
Nominal length	60–9000 mm	120–9000 mm
Air pressure (max.)	600 kPa	600 kPa
Frequency (max.)	3 Hz	2 Hz
Tensile force (max. at 600 kPa)	1500 N	6000 N
Permissible freely suspended load	80 kg	250 kg
Permissible pre-tensioning	0.04·Nominal length	0.05·Nominal length
Permissible contraction	0.25·Nominal length	0.25·Nominal length
Permissible working temperature	–5 … +60 °C	–5 … +60 °C
Fitting size	M10×1.25–M20×1.5	M16×1.5–M30×1.5
Weight	169 g + 178 g/m	675 g + 340 g/m

The schematic for the formation of the pressing force and scaled CAD drawing are given in **Figure 4**. In this figure, F_{pam} is the tensile force of the PAM, F_n is the normal force to the joint, F_r is the perpendicular force to the vertical axis of the clamping system, F_a is the clamping arm force, F_p is the pressing force, β is the angle of the cam block, α is the angle between the arms and the vertical axis, and i is the reduction ratio of the press mechanism. The mathematical formulation depending on this notation is expressed by Equations (13) – (17) as follows:

$$F_n = F_{pam} \cos\beta \tag{13}$$

$$F_r = F_{pam} \cos\beta \sin\beta \tag{14}$$

$$F_a = \frac{F_r}{\sqrt{2\cdot(1+\cos(180-2\alpha))}} \tag{15}$$

$$F_p = \frac{2F_{pam} \cos\beta \sin\beta \cos\alpha}{\sqrt{2\cdot(1+\cos(180-2\alpha))}} \tag{16}$$

$$i = \frac{2\cos\beta \sin\beta \cos\alpha}{\sqrt{2\cdot(1+\cos(180-2\alpha))}} \tag{17}$$

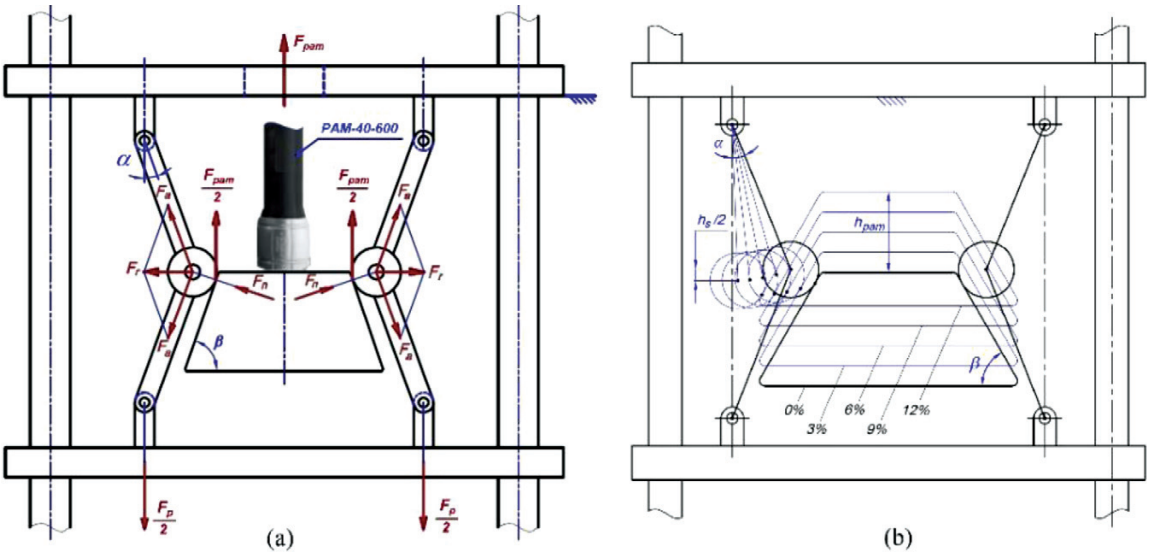

Figure 4: a) Schematic for the generation of the pressing force, b) scaled CAD drawing

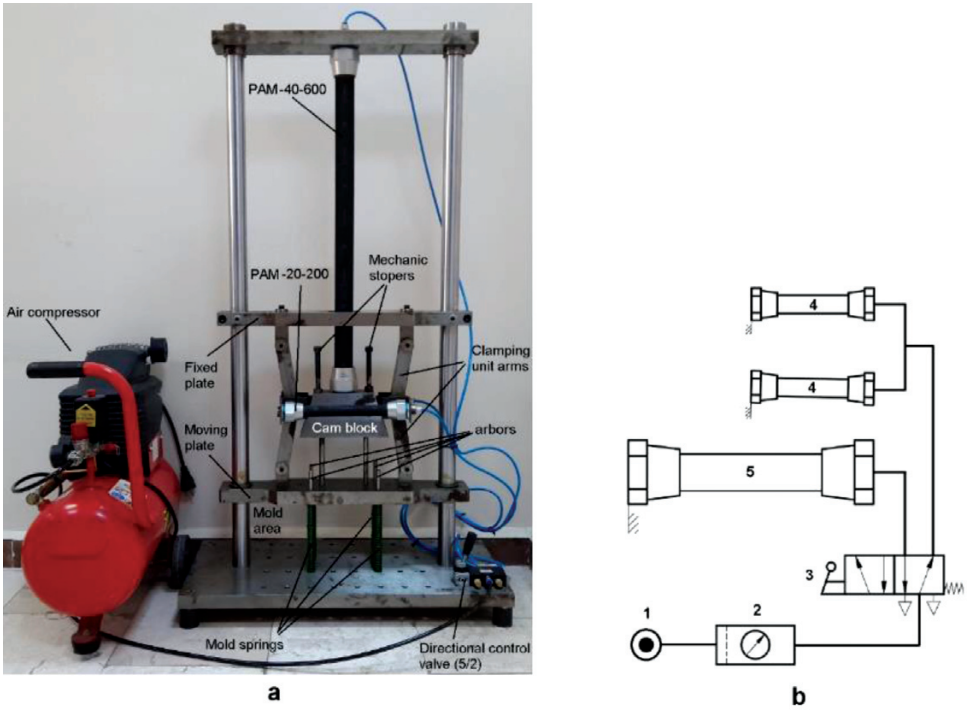

Figure 5: PAM-based press: a) general view, b) pneumatic circuit diagram (1: air compressor, 2: manometer-filter, 3: 5/2 directional control valve, 4: PAM–20–200, 5: PAM–40–600)

The press was manufactured after the optimization of the main dimensions and the sizing calculations of the components. The diameter of the pins and the thickness of the fixed and moving plates were determined as 16 mm and 30 mm. The maximum deformation at the plates was found to be 0.14 mm in the deformation analysis. Modeling and design-validation studies according to the sizes obtained in the calculations, material supply, manufacturing, and assembly works were carried out. The general view of the developed system and pneumatic circuit diagram are shown in **Figure 5**. The pneumatic circuit consists of the air compressor, manometer, 5/2 lever-operated directional control valve, one PAM for main press force, and two PAMs for bringing back the press to the neutral position. The nominal operating pressure, tank volume, and flow rate of the air compressor are 800 kPa, 24 L, and 198 L/min, respectively.

3 RESULTS AND DISCUSSION

The force graphs obtained in the experimental studies carried out are given in Figure 6. It is observed that the tensile force generated by the PAM is directly proportional to the air pressure and the initial cross-sectional area. It is the function of the stroke resulting from the change in fiber orientation. Contraction rates below 12 % provide an effective working range, and due to that the working efficiency increases as the contraction rate becomes smaller. In this operating range the force varies as 1606–682 N for PAM-20-200 and 6321–3071 N for PAM-40-600. At the initial state, the contraction ratio is zero, and the force has its maximum value.

Conversely, the contraction ratio reaches its maximum value, while the force decreases to zero at the final

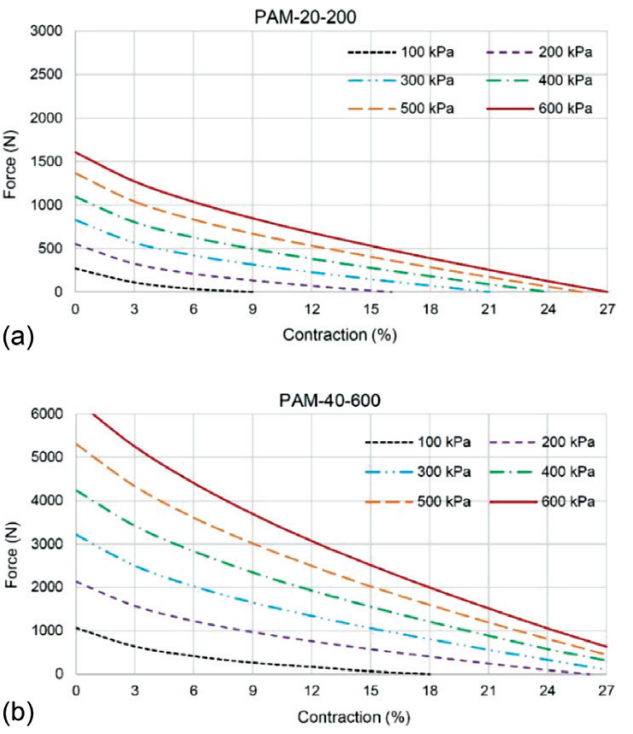

Figure 6: Tensile forces of the PAMs used: a) PAM–20–200, b) PAM–40–600

Table 2: Experimental results obtained at 200 kPa, 400 kPa and 600 kPa air pressure for PAM-40-600.

Pressure p (kPa)	Arm angle α (deg)	PAM stroke h_{pam} (mm)	PAM stroke h_{pam} (%)	PAM force F_{pam} (N)	Displacement h_s (mm)	Reduction ratio	Press force F_p (N)
200	22	0	0	2130	0	1.07	2283
	16.35	18	3	1569	9.06	1.48	2316
	11.26	36	6	1221	15	2.17	2656
	6.52	54	9	968	18.58	3.79	3667
	2.06	72	12	757	20.2	12.04	9113
400	22	0	0	4240	0	1.07	4544
	16.35	18	3	3422	9.06	1.48	5051
	11.26	36	6	2832	15	2.17	6159
	6.52	54	9	2340	18.58	3.79	8865
	2.06	72	12	1923	20.2	12.04	23149
600	22	0	0	6321	0	1.07	6774
	16.35	18	3	5248	9.06	1.48	7746
	11.26	36	6	4405	15	2.17	9580
	6.52	54	9	3693	18.58	3.79	13991
	2.06	72	12	3071	20.2	12.04	36969

state. The decrease of the force gives smoothness to the movement. In contrast to this, pneumatic cylinders produce the same force throughout their entire stroke and require cushioning at the end of the stroke to avoid the impact effect when the speed is suddenly reset to zero. The PAM behaves like a spring and follows the application of force when the external force changes. Both the pre-tensioning force and the spring stiffness of this pneumatic spring can be varied. Operational situations such as a constant-pressure or constant-volume spring provide suitable properties.

The results obtained from press tests are listed in **Table 2**. Among the values in this table, the clamping-arm angle, PAM stroke, and displacement were determined by the scaled CAD drawing in **Figure 4b**. The pressing forces and reduction ratios were determined by Equations (16) and (17) according to the angles (α, β) and PAM forces.

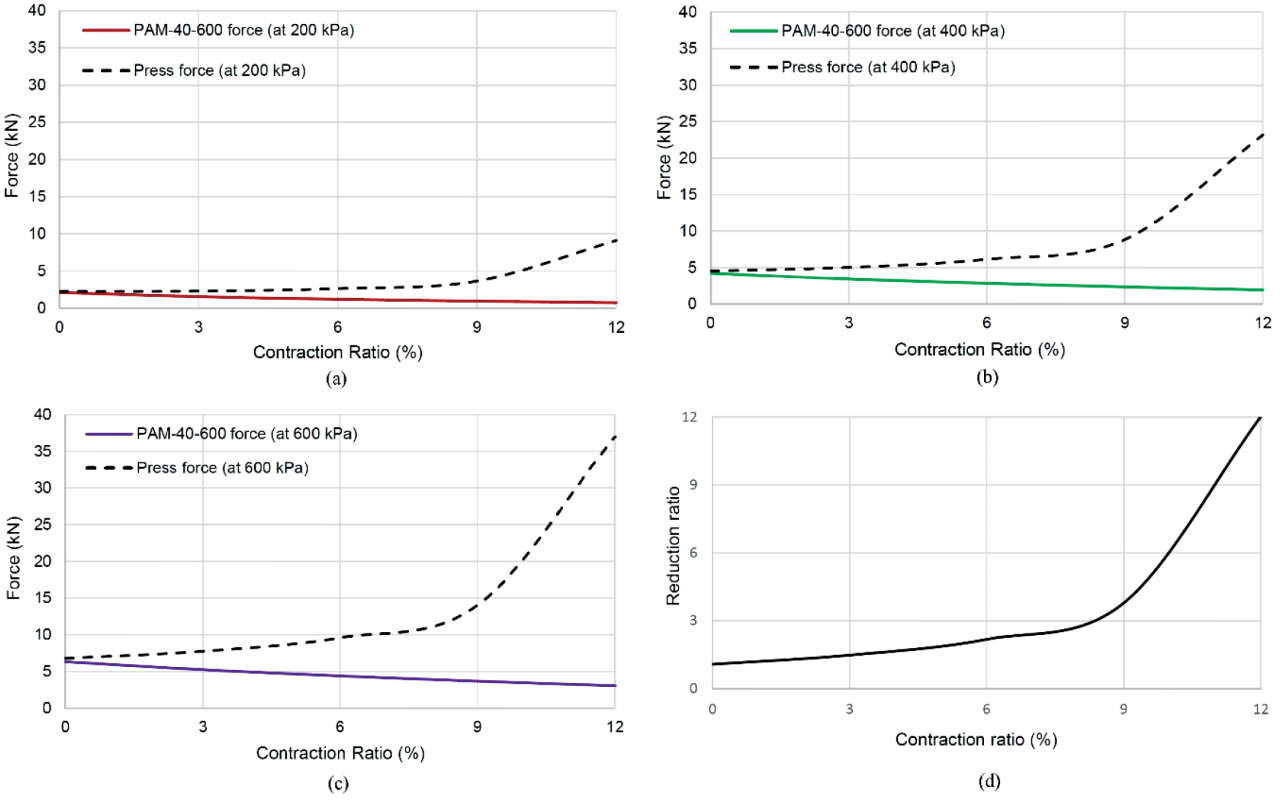

Figure 7: Tensile forces of PAM–40–600 and the pressing forces at: a) 200 kPa, b) 400 kPa, c) 600 kPa, d) reduction ratio of the press mechanism

The clamping system used in the design makes up a reduction effect that increases the pressing force. The reduction ratio increases as the α angle of the clamping arms with the vertical axis increase. **Figure 7a** to **7c** shows the pulling force produced by the PAM-40-600 and the pressing force obtained when (200, 400 and 600) kPa of air pressure is applied, respectively. According to these results, it can be said that the pressing forces of (9.1, 23.1, and 36.9) kN are obtained by using a single 40-mm-diameter PAM. When these figures are examined, the muscle produces the maximum pulling force at the beginning, and this force decreases towards the end of the stroke. This is in line with the characteristic way of working of the muscle. Since the sheet-metal forming process takes place at the end of the stroke, the force drop towards the end of the stroke is not a desirable situation. On the other hand, the press mechanism comes into play at this stage. There is a radical increase in the pressing force, while the pulling force of the muscle decreases. The pressing-force graphs in these figures indicate that the most suitable region for punching the sheet metal is the contraction range 9–12 %. It is desirable in the case of sheet-metal cutting and punching molds because the press moves freely at first and does the work when it comes to the stroke end. In addition, while the tensile force of the PAM is reduced with the stroke, this reduction effect of the clamping system acts to balance the force. **Figure 7d** shows the reduction ratio change concerning the contraction of PAM-40-600.

In presses where pneumatic and hydraulic cylinders are used, the pressing force and velocity at a certain pressure are fixed throughout the stroke. Here, in contrast, the pressing force and velocity are variable throughout the stroke. Because the tensile force of the PAM is variable depending on the stroke and the clamping system's reduction effect. In addition, the cam block geometry is an effective parameter. In the case of a linear cam-block geometry, the pressing characteristic can be controlled via its angle and height. The case of a curvilinear cam-block geometry will further enhance the control flexibility of the system.

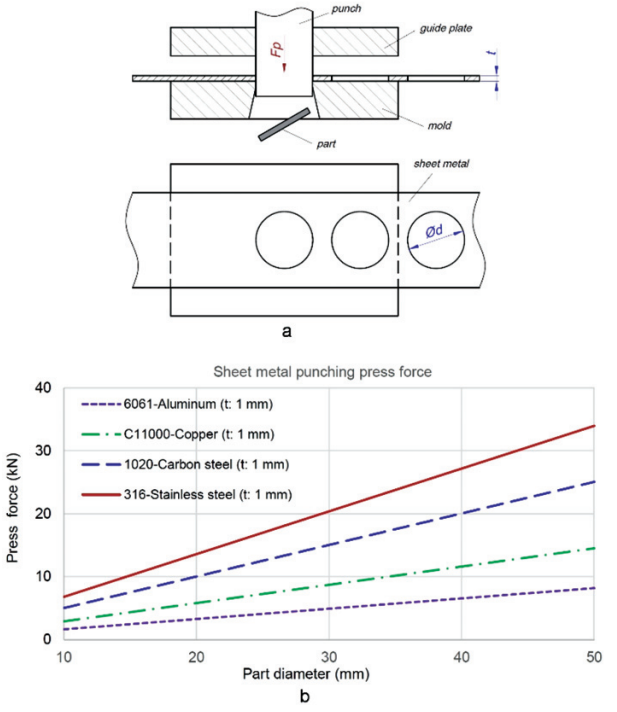

Figure 8: Pressing force during sheet-metal punching: a) schematic, b) press force requirements

The desired final metal parts are obtained by applying cutting, punching, bending, and forming processes to sheet metals in mechanical and hydraulic presses. **Figure 8a** shows a schematic of the sheet-metal punching procedure. In punching molds, the elasticity limit of the sheet material is exceeded by the punch force, and plastic deformation begins. As the punch plunges into the material up to 0.3 times the thickness, the part starts to flow toward the lower mold cavity. When 0.6 times the sheet thickness is reached, the cutting process is completed, and the part is pushed and dropped from the mold cavity.

The parameters that determine the pressing-force requirement are the shear strength of the material, the sheet thickness, and the length of the cutting contour. Depending on these parameters, the pressing force required for a circular part is expressed by Equation (18) as follows:

$$F_{\mathrm{p}} = \pi \cdot d \cdot t \cdot R_{\mathrm{m}} \cdot c \tag{18}$$

where d, t, R_{m} and c are the diameter of the circular part, the thickness of the sheet metal, the tensile strength of the material, and the processing coefficient, respectively. To show the suitability of the pressing force obtained by PAM-40-600 for thin sheet-metal parts ($t < 1$ mm), pressing-force calculations were made for commonly used metals. Tensile strengths of the 6061–annealed aluminum, C11000–hot-rolled copper, 1020–hot-rolled carbon steel, and 316–annealed stainless steel are considered as 124, 220, 380, and 515 MPa, respectively.[24]

The force required for sheet-metal forming is a function of the cut-to-length of the part, the thickness of the sheet metal, and the tensile strength of the material. As the diameter and thickness of a circular part and the tensile strength of the material increase, the required forming force also increases. **Figure 8b** shows the sheet-forming forces needed for circular parts with a wall thickness of 1 mm and a diameter of 10–50 mm made of the above-mentioned materials. When the figure is examined, it is seen that the required force for the circular part with a wall thickness of 1 mm and a diameter of 50 mm, which is made of annealed 316 stainless steel with the highest tensile strength among the above-mentioned materials, is 33.9 kN. The obtained results given in **Figure 8b** show that the pressing force obtained by a single PAM-40-600 is sufficient for thin sheet-metal punching molds.

4 CONCLUSIONS

The design, manufacturing, and test studies of a press actuated with three PAMs were carried out. The PAMs are suitable for generating the pressing force, besides the robotic, prosthetic, and biomimetic applications. At the end of the study, a prototype of the PAM-based press was developed as an alternative approach to hydraulic and mechanical presses. It can be used for a more precise determination of the areas where the PAM-based systems can be operated and in which design changes can be made in accordance with the requirements and adaptations to the related sectors. Since the PAM is a hermetically sealed system and not equipped with any moving components, it is possible to operate the developed system in dirty and dusty environments and even in water. The production cost is lower because of the relatively cheap pneumatic circuit elements. Although the PAM-based studies cover many areas, such as manipulators, automation systems, robotic actuators, and prosthetic assistive devices, there is no study on presses with PAMs in the literature.

This study shows that a sufficient level of pressing force can be obtained with a single pneumatic artificial muscle to form thin sheet metals and fills the gap in the related literature. The force-enhancing effect of the press mechanism compensates for the decrease in the tensile force of the pneumatic artificial muscle as the contraction rate increases. It is suitable because the pressing force increases, and the speed decreases during punching at the end of the stroke. The results show that pressing forces of (9.1, 23.1, and 36.9) kN are obtainable by using a single 40-mm-diameter PAM at (200, 400, and 600) kPa air pressures, respectively.

Acknowledgment

This work was supported by TUBITAK, The Scientific and Technological Research Council of Turkey [grant number 122M619].

5 REFERENCES

[1] X. Zhu, G. Tao, B. Yao, J. Cao, Adaptive robust posture control of a parallel manipulator driven by pneumatic muscles, Automatica, 44 (**2008**) 9, 2248–2257, doi:10.1016/j.automatica.2008.01.015

[2] K. K. K. Ku, R. S. Bradbeer, K. K. Y. Lam, L. F. Yeung, R. C. W. Li, A novel actuator for underwater robots, IEEE J. Ocean. Eng., 34 (**2009**) 3, 331–342, doi:10.1109/JOE.2009.2014928

[3] K. Harihara, S. Dohta, T. Akagi, F. Zhang, Development of a search type rescue robot driven by pneumatic actuator, in: SICE Annual Conf., Taipei, Taiwan, (**2010**) 1311–1317, doi:10.1299/jsmecs.2010.48.303

[4] A. Bleicher, T. Schauer, M. Valtin, J. Raisch, M. Schlaich, Active vibration control of a light and flexible stress ribbon footbridge using pneumatic muscles, in: IFAC Annual Conf., Milano, Italy, (**2011**), 911–916, doi:10.3182/20110828-6-IT-1002.02781

[5] T. Kishi, T. Nakamura, M. Ikeuchi, Development of a peristaltic crawling inspection robot with pneumatic artificial muscles for a 25A elbow pipe, Nature-Inspired Mobile Robotics, (**2013**), 301–308, doi:10.1142/9789814525534_0039

[6] G. Soy, G. Samtas, S. Korucu, Design and evaluation of pneumatic movement mechanism supported with solar panels, J. Polytech., 17 (**2014**), 135–142, doi:10.2339/2014.17.3 135-142

[7] T. Leephakpreeda, Mathematical modeling of pneumatic artificial muscle actuation via hydrogen driving metal hydride-$LaNi_5$, J. Bionic Eng., 9 (**2012**) 1, 110–118, doi:10.1016/S1672-6529(11)60103-0

[8] T. Nuchkrua, T. Leephakpreeda, Actuation of pneumatic artificial muscle via hydrogen absorption/desorption of metal hydride-$LaNi_5$, Adv. Mech. Eng., 7 (**2015**) 1, 364306, doi:10.1155/2014/364306

[9] T. Nuchkrua, T. Leephakpreeda, Novel Compliant Control of a Pneumatic Artificial Muscle Driven by Hydrogen Pressure Under a Varying Environment, IEEE Trans. Ind. Electron., 69 (**2022**) 7, 7120–7129, doi:10.1109/TIE.2021.3102486

[10] T. Nuchkrua, T. Leephakpreeda, T. Mekarporn, Development of robot hand with Pneumatic Artificial Muscle for rehabilitation application, in: NANOMED Annual Conf., Phuket, Thailand, (**2013**), 55–58, doi:10.1109/NANOMED.2013.6766315

[11] A. Hošovský, J. Pitel, K. Židek, J. Sárosi, L. Cveticanin, Dynamic characterization and simulation of two-link soft robot arm with pneumatic muscles, Mech. Mach. Theory, 103 (**2016**), 98–116, doi:10.1016/j.mechmachtheory.2016.04.013

[12] A. Merola, D. Colacino, C. Cosentino, F. Amato, Model-based tracking control design, implementation of embedded digital controller and testing of a bio-mechatronic device for robotic rehabilitation, Mechatronics, 52 (**2018**), 70–77, doi:10.1016/j.mechatronics.2018.04.006

[13] T. Wang, X. Chen, W. Qin, A novel adaptive control for reaching movements of an anthropomorphic arm driven by pneumatic artificial muscles, Appl. Soft. Comput., 83 (**2019**), 105623, doi:10.1016/j.asoc.2019.105623

[14] G. V. Prado, M. B. C. Sanchez, Control strategy of a pneumatic artificial muscle for an exoskeleton application, IFAC Papers OnLine, 52 (**2019**), 281–286, doi:10.1016/j.ifacol.2019.06.075

[15] T. C. Tsai, M. H. Chiang, Design and control of a 1-DOF robotic lower-limb system driven by novel single pneumatic artificial muscle, Appl. Sci., 43 (**2020**) 1, 1–21, doi:10.3390/app10010043

[16] B. Kalita, S. K. Dwivedy, Nonlinear dynamic response of pneumatic artificial muscle: A theoretical and experimental study, Int. J. Non-Linear Mech., 125 (**2020**), 103544, doi:10.1016/j.ijnonlinmec.2020.103544

[17] G. Zhong, Y. Hou, W. Dou, A soft pneumatic dexterous gripper with convertible grasping modes, Int. J. Mech. Sci., 153 (**2019**), 445–456, doi:10.1016/j.ijmecsci.2019.02.028

[18] G. Zhong, W. Dou, X. Zhang, H. Yi, Bending analysis and contact force modeling of soft pneumatic actuators with pleated structures, Int. J. Mech. Sci., 193 (**2021**), 106150, doi:10.1016/j.ijmecsci.2020.106150

[19] W. Xiao, X. Du, W. Chen, G. Yang, D. Hu, X. Han, Cooperative collapse of helical structure enables the actuation of twisting pneumatic artificial muscle, Int. J. Mech. Sci., 201 (**2021**), 106483, doi:10.1016/j.ijmecsci.2021.106483

[20] C. P. Chou, B. Hannaford, Measurement and modeling of McKibben pneumatic artificial muscles, IEEE Trans. Robot. Autom., 12 (**1996**) 1, 90–102, doi:10.1109/70.481753

[21] M. Martens, I. Boblan, Modeling the static force of a Festo pneumatic muscle actuator: A new approach and a comparison to existing models, Actuators, 6 (**2017**) 4, 1–11, doi:10.3390/act6040033

[22] B. Tondu, P. Lopez, Modeling and control of McKibben artificial muscle robot actuators, IEEE Control Syst. Mag., 20 (**2000**) 2, 15–38, doi:10.1109/37.833638

[23] K. C. Wickramatunge, T. Leephakpreeda, Study on mechanical behaviors of pneumatic artificial muscle, Int. J. Eng. Sci., 48 (2010) 2, 188–198, doi:10.1016/j.ijengsci.2009.08.001

[24] W. D. Callister, D. G. Rethwisch, Materials science and engineering, 8th ed., Wiley, (2011)